Original research article

Sex Differences in Right Ventricular Adaptation to Pressure Overload in a Rat Model

Tik-Chee Cheng[1], Diana M. Tabima[1], Laura Caggiano[2], Andrea L. Frump[3], Timothy A. Hacker[4], Jens C. Eickhoff[5], Tim Lahm[3,6,7], Naomi C. Chesler[1,2,8]

Affiliations:
[1]Department of Biomedical Engineering, University of Wisconsin-Madison, Madison, WI
[2]University of California, Irvine Edwards Lifesciences Foundation Cardiovascular Innovation and Research Center, Irvine, CA
[3]Department of Medicine; Division of Pulmonary, Critical Care, Sleep and Occupational Medicine, Indiana University School of Medicine, Indianapolis, IN
[4]Cardiovascular Physiology Core Facility, University of Wisconsin-Madison School of Medicine and Public Health, Madison, Wisconsin
[5]Department of Biostatistics and Medical Informatics, University of Wisconsin-Madison, Madison, WI
[6]Division of Pulmonary, Critical Care and Sleep Medicine, National Jewish Health, Denver, CO
[7]Richard L. Roudebush VA Medical Center, Indianapolis, IN
[8]Department of Biomedical Engineering, University of California, Irvine (UCI), Irvine, CA

Corresponding author:

Naomi C. Chesler, PhD
Director, UCI Edwards Lifesciences Foundation Cardiovascular Innovation and Research Center
Professor, Department of Biomedical Engineering
2420 Engineering Hall
Irvine, CA 92697-2700
E-mail: nchesler@uci.edu
Telephone number: (608) 215-7565

Running head: Sex Differences in RV adaptation

Keywords: sex difference, ovariectomy, mechanical efficiency, mechanoenergetic cost

Abstract

With severe right ventricular (RV) pressure overload, women demonstrate better clinical outcomes compared to men. The mechanoenergetic mechanisms underlying this protective effect, and their dependence on female endogenous sex hormones, remain unknown. To investigate these mechanisms and their impact on RV systolic and diastolic functional adaptation, we created comparable pressure overload via pulmonary artery banding (PAB) in intact male and female Wistar rats and ovariectomized females (OVX). At 8 weeks post-surgery, right heart catheterization demonstrated increased RV energy input (indexed pressure-volume area; iPVA) in all PAB groups, with the greatest increase in intact females. PAB also increased RV energy output (indexed stroke or external work; iEW) in all groups, again with the greatest increase in intact females. In contrast, PAB only increased RV contractility (indexed end systolic elastance, iE_{es}) in females. Despite these sex-dependent differences, there were no statistically significant effects observed in the ratio of RV energy output to input (mechanical efficiency) or in mechanoenergetic cost to pump blood with pressure overload. These metrics were similarly unaffected by loss of endogenous sex hormones in females. Also, despite sex-dependent differences in collagen content and organization with pressure overload, decreases in RV compliance and relaxation time constant (Tau Weiss) were not determined to be sex-dependent. Overall, despite sex-dependent differences in RV contractile and fibrotic responses, RV mechanoenergetics for this degree and duration of pressure overload are comparable between sexes and suggest a homeostatic target.

New and Noteworthy

Sex differences in right ventricular mechanical efficiency and energetic adaptation to increased right ventricular afterload were measured. Despite sex-dependent differences in contractile and fibrotic responses, right ventricular mechanoenergetic adaptation was comparable between the sexes, suggesting a homeostatic target.

Introduction

Sex differences influence the progression of right ventricular failure (RVF) secondary to pressure overload, which is the primary cause of death in patients with pulmonary arterial hypertension, pulmonary hypertension secondary to left heart disease, and chronic thromboembolic pulmonary hypertension(13). In both the healthy and pressure overloaded RV, women demonstrate superior RV systolic and diastolic function(10, 16, 45, 50, 53), which contributes to their better adaptation and survival to pulmonary hypertension (PH)(16). Moreover, some of these sex differences in RV function with PH diminish with age(54, 56), which implicates age-related (i.e., menopausal) loss of endogenous sex hormone signaling in adaptive RV remodeling to pressure overload. Some experimental studies in rodent models of PH similarly have demonstrated superior female RV function(11, 25) and dependence on endogenous estrogen(25); however, some of these studies may have been confounded by sex differences in PH severity and RV afterload. A better understanding of the pathophysiological mechanisms underlying sex differences in the pressure overloaded RV is critical to treatment and management of RVF.

Cardiac mechanics, energy utilization, and their interactions are important clinical contributors to systolic and diastolic adaptation to pressure overload(1, 18, 21, 29, 36, 37). Pressure overload increases RV wall tension such that the hemodynamic energy output generated by the RV in maintaining cardiac output is increased(32, 52, 55). To decrease wall tension, the RV undergoes hypertrophy and wall thickening, which lead to an adaptive increase in RV contractility(32). In the adapted RV, increased energy output is met with proportional increase in energy input(46). With disease progression, however, the RV myocardium undergoes additional remodeling processes, such as wall thinning and fibrosis, that impair the maintenance of enhanced RV

contractility, and the RV begins to fail, which is evidenced by reduced cardiac output(55). During this stage, hemodynamic energy output is insufficient despite energy input, such that mechanical efficiency is reduced(5).

Mechanical efficiency, which is the ratio of energy output to energy input, is a holistic metric of ventricular function(42). Another, more novel, metric is the mechanoenergetic cost to pump blood(21), which is a function of ventricular afterload, (E_a), end systolic elastance (E_{es}), and stroke volume. As defined mathematically by Kawaguchi et al., the mechanoenergetic cost to pump blood increases with E_a, because pressure overload raises myocardial oxygen consumption(21), and with E_{es}, because increased contractility increases oxygen consumption(35). This mechanoenergetic cost is sustained by metabolic energy generated by proper mitochondrial function(24, 46, 47). Interestingly, patients with heart failure with preserved ejection fraction demonstrate greater mechanoenergetic cost to deliver blood compared to age- and blood pressure-matched controls(21). Moreover, diastolic dysfunction increased with increased mechanoenergetic cost to pump blood(21).

The impacts of sex differences and endogenous female sex hormones on mechanical efficiency and mechanoenergetic cost to pump by the RV are unknown. We have previously shown that repletion of the female sex hormone estrogen increases mechanical efficiency in ovariectomized female rats with Sugen/hypoxia-induced pulmonary hypertension (SuHx-PH)(27), and that the response of both the pulmonary vasculature and RV to SuHx is sex-dependent(11, 25). To investigate the impact of sex and loss of endogenous female sex hormones on RV mechanics and energetics under comparable pressure overload conditions, we used a pressure overload model in

which the degree of afterload increase (induced by pulmonary artery banding; PAB) was normalized to the different body sizes in male and female animals. This approach generated comparable RV pressure overload in intact males and females as well as ovariectomized females (OVX), which we then used to investigate the sex- and female sex hormone-dependent mechanoenergetic adaptation of the RV to pressure overload.

Methods

Animal studies

A total of 36 8-week-old female Wistar rats (Charles River, Wilmington, MA) were used in this study, 18 of which were ovariectomized (OVX) and 18 of which remained intact. Animals were ovariectomized between 6 and 7 weeks of age (week -1). At week 0, all animals underwent a thoracotomy in which the main pulmonary artery (PA) diameter was directly measured using a spring divider and calipers. Animals were then randomly assigned to undergo either PAB (OVX: n = 8, Intact: n = 9) or sham surgery (Sham, OVX: n = 10, Intact: n = 9; see below for details). All animals were monitored weekly for signs and symptoms of RV failure including dyspnea, palpable ascites, inactivity, and ruffled fur(4, 5) until 8 weeks post-surgery. OVX rats were fed a soybean-free chow (Teklad 2020x, Envigo, Indianapolis, IN) during the entire study to preclude potential confounding effect of dietary endogenous hormones. At the terminal time point, we confirmed the lack of ovaries in OVX rats. To assess RV-specific sex differences in the setting of PAB, we compared the resulting hemodynamic, biochemical, and histological data to those collected in male Wistar rats (Sham: n = 9, PAB: n = 10) published previously(5) in which identical surgical, animal care, and measurement procedures were used. A timeline and overview

of the experimental groups is provided in Fig. 1. All animal experiments were reviewed and approved by the University of Wisconsin Institutional Animal Care and Use Committee.

Pulmonary artery banding and sham surgery

PAB and sham surgeries were performed through a lateral thoracotomy and dissection of the main PA as described before(5). Briefly, rats were anesthetized with isoflurane (5% and then maintained at 2-3%, balance oxygen), intubated, and ventilated. Rats randomly assigned to the PAB group had a silk suture tied around the main PA and a reference needle to achieve approximately 60-70% constriction based on the direct measurement of the PA. Rats assigned to the Sham group did not have the PA suture tied in place. Rats were monitored weekly for bodyweight (BW) changes and appearance for up to 8 weeks post-surgery.

Pressure-volume measurements

Terminal invasive right heart catheterization was performed to assess RV function as previously described(5). Rats were anesthetized with urethane (1.6 kg/g, i.p.), intubated, and ventilated. Systemic pressure was measured using a pressure catheter (Millar, Houston, TX) positioned at the aortic arch inserted through the right carotid artery. RV pressure and volume (PV) were measured using a 1.9F 6 mm spacing PV catheter (Transonic Scisense, London, Ontario, Canada) inserted into the RV through the apex of the heart after removal of the chest wall. Measurements were recorded on Notocord Systems (Croissy Sur Seine, France). After baseline

recordings, at least 3 inferior vena cava (IVC) occlusions were performed to obtain end systolic PV relationships.

Terminal surgery

Two OVX PAB rats did not survive urethane anesthesia; post-mortem examination indicated significant abdominal fluid and hypertrophied right atria (139.6 ± 26.2 mg OVX PAB vs. 38.1 ± 3.0 mg OVX Sham). Also, one of these two rats had significant liver discoloration and enlargement, suggestive of hepatic congestion. Tissues from these two rats were harvested and included in RV hypertrophy calculation, histology, and biochemical assays but no hemodynamic data could be collected.

Pressure-volume calculations

Using RV PV waveforms, baseline hemodynamic endpoints were determined, including RV end-systolic pressure (Pes), end-diastolic pressure (Ped), end-diastolic volume (Ved), end-systolic volume (Ves), and isovolumic relaxation time constant (tau Weiss). In cases where PV loop distortion occurred, Ved was taken as the midpoint between the maximum and minimum values recorded during isovolumic contraction. E_{es} was determined from calculating the slope of end-systolic pressure volume relationship measured during IVC occlusion. E_a, a measurement of RV afterload, was calculated by taking the ratio of Pes and stroke volume (SV). Due to significant bodyweight differences between females and males (Table 1), volume-based metrics were indexed to terminal bodyweight to better reflect differences in the RV and arterial properties with

sex and loss of endogenous sex hormones. Indexed parameters include end-systolic volume (iVes), end-diastolic volume (iVed), stroke volume (stroke volume index; SVI), cardiac output (cardiac index; CI), RV chamber compliance ($\Delta V/\Delta P$), iE_a, iE_{es} (derived from vena cava occlusions), external work (iEW, energy output), and pressure volume area (iPVA, energy input). EW, calculated using the product of SV and right ventricular end systolic pressure (Pes), is an estimate of the mechanical energy used during contraction, while PVA is a measure of total mechanical energy generated during a cardiac cycle(40). RV mechanical efficiency was assessed as iEW/iPVA(33, 48, 49).

Model-based prediction of RV mechanoenergetic cost to pump blood

To describe ventricular adaptation, we used a model developed previously by Kawaguchi *et al.*(21). Briefly, the mechanoenergetic cost to deliver blood is defined mathematically as the differential change in PVA with respect to SV or $\left(\frac{\partial(\boldsymbol{PVA})}{\partial(SV)}\right)$. Like the measured PVA, this continuously differential form of PVA, which we denote ***PVA***, includes both productive work (stroke work; SW) and non-productive work (potential energy; PE = ***PVA*** – SW). If the change in ***PVA*** per unit SV increases, the cost to deliver a given amount of blood increases. If the ***PVA*** stays constant as SV increases, the cost to deliver blood decreases. To define the dependence of ***PVA*** on SV such that $\left(\frac{\partial(\boldsymbol{PVA})}{\partial(SV)}\right)$ can be derived, the following relationships are used per(20, 22, 48, 49):

$$Pes = \frac{iE_a \times SV}{BW} \quad \text{(Eqn. 1)}$$

$$Pes = \frac{iE_{es}(Ved - SV - V_0)}{BW} \quad \text{(Eqn. 2)}$$

where V_0 is the volume axis intercept of the end-systolic pressure volume relation. These equations are first rearranged to compute SV in terms of iE_{es} and iE_a:

$$SV = \frac{iE_{es}(Ved - V_0)}{iE_{es} + iE_a} \quad \text{(Eqn. 3)}$$

And then, given the following defining equations:

$$\boldsymbol{PVA} = SW + PE \quad \text{(Eqn. 4)}$$

$$SW = Pes \times SV \quad \text{(Eqn. 5)}$$

we can obtain an expression for PE in terms of Pes and E_{es}:

$$PE = \frac{(P_{es})^2 \times BW}{2 \times iE_{es}} \quad \text{(Eqn. 6)}$$

Such that ***PVA*** can be expressed in closed form as a function of SV(33, 46, 48, 49):

$$\boldsymbol{PVA} = \frac{1}{2}\frac{iE_a}{BW}SV^2 + \frac{1}{2}\frac{iE_a \times Ved}{BW}SV - \frac{1}{2}\frac{iE_a \times V_0}{BW}SV \quad \text{(Eqn. 7)}$$

Finally, this expression for ***PVA*** can be differentiated with respect to SV and expressed in terms of iE_{es} and iE_a to obtain:

$$\frac{\partial(\boldsymbol{PVA})}{\partial(SV)} = \frac{iE_a(Ved - V_0)}{BW}\left(\frac{iE_{es}}{iE_{es} + iE_a} + \frac{1}{2}\right) \quad \text{(Eqn. 8)}$$

Note that the final expression for $\left(\frac{\partial(\boldsymbol{PVA})}{\partial(SV)}\right)$ is independent of measured SV, although dependent on Ved-V_0.

This expression for the mechanoenergetic energy cost to pump blood was calculated for each animal. The results were plotted on a 3D surface with iE_{es} as the x-axis, iE_a as the y-axis, and

$\left(\frac{\partial(\boldsymbol{PVA})}{\partial(SV)}\right)$ as the z-axis with the average value for each experimental group the centroid of an elliptical surface and the boundary defined by the standard error of mean.

17β-estradiol serum concentration measurement

Following hemodynamic data collection, rats were euthanized and ~1.5 mL of blood was collected. Blood samples were spun at 4,000 rpm for 10 min at 4C, aliquoted, and stored in -80C. Serum samples were thawed on ice for 17β-estradiol measurement using Calbiotech Mouse/Rat Estradiol ELISA kit (El Cajon, CA) according to manufacturer's instructions and as performed previously(11).

Gross histologic evaluation

After blood was collected, the heart was excised. RV free wall was separated from the LV and septum and weighed. RV hypertrophy was calculated as the RV weight scaled to the sum of LV and septal weights (Fulton index). The RV was sectioned for further histological and biochemical assessments. Post-mortem evaluation confirmed the absence of ovaries and a shrunken uterus in all OVX female rats.

Histology and image analysis

A section of RV was fixed in 10% v/v formalin, preserved in 70% ethanol, embedded in paraffin, sectioned, and stained with hematoxylin and eosin to visualize cardiomyocytes(56) or picrosirius

red to visualize collagen(5). RV cardiomyocytes were identified and cross-sectional area (CSA) was manually measured using ImageJ (version 1.49v, National Institutes of Health, Bethesda, MD) in at least four representative fields of view. Collagen deposition in the RV was identified by color thresh-holding using MetaVue (Optical Analysis Systems) in at least nine representative images. To quantify overall percentage of collagen content, the area containing interstitial collagen was divided by the tissue area in each field of view. Thick, tightly packed collagen and thin, loosely aligned collagen were identified as different interference colors under polarized light, with thick collagen defined as red, orange, or yellow color, and thin collagen as green color(3, 19, 30). The ratio of thick to thin collagen fiber bundles was calculated for each image and averaged to obtain a single measurement for each rat. All histological analyses were performed by two observers blinded to sex and experimental condition.

Real time reverse transcriptase polymerase chain reaction analysis

RNA was extracted from 10-15 mg of RV using Qiagen RNeasy Fibrous Tissue Mini Kit (Valencia, CA). Total RNA was recovered with A260/280 nm ranging from 1.85 to 2.10. 900 ng of RNA was reverse transcribed into cDNA using Applied Biosystems High Capacity cDNA Reverse Transcription Kit (Foster City, CA). Real-time RT PCR was performed using TaqMan Gene Expression Master Mix (Invitrogen Life Technologies, Carlsbad, CA). TaqMan assay primers included the following: peroxisome proliferator-activated receptor gamma coactivator 1 alpha (PGC-1α) (*Ppargc1*; Rn00580241_m1), estrogen receptor alpha (ERα) (*Esr1*; Rn01640372_m1), estrogen receptor beta (ERβ), (*Esr2*; Rn00562610_m1), G-protein coupled estrogen receptor (GPR30) (*Gper1*; Rn00592091_s1), and hypoxanthine

phosphoribosyltransferase 1(*Hprt1*; Rn01527840_m1). 10 ng of cDNA was used to measure PGC-1α mRNA expression while 50 ng was used to measure *Esr1*, *Esr2*, and *Gper1* on the Applied Biosystems StepOne Plus Real-Time PCR System. Changes in mRNA expression were determined by the comparative threshold cycle (ΔΔCT) method(28). Data were normalized to Hprt1 and expressed as fold change compared to the intact female sham group.

Electron microscopy and mitochondrial ultrastructure image analysis

A section of the RV was immersed in cold Karnovsky's fixative (Electron Microscopy Sciences, Hatfield, PA) and processed for transmission electron microscopy to assess mitochondrial ultrastructure(5). For each rat RV, at least four images were acquired and analyzed using ImageJ. Mitochondrial content was reported as the average numbers of mitochondria counted per animal. Mitochondrial size was reported as the average cross-sectional area of contoured mitochondria per animal. These analyses were performed by a blinded observer.

Statistical analysis

All values are presented as mean ± standard error, stratified by exposure groups and sex. Two-factorial analysis of variance (ANOVA) to determine differences in hemodynamic, biochemical, and histological outcome parameters due to PAB (Sham vs. PAB), sex (Intact male vs. Intact female or OVX female), and female sex hormone-depletion (Intact female vs. OVX female). Normal probability plots were examined to evaluate the normality assumption. If there was indication for unequal variances and/or violation of normality for an outcome variable, then the outcome variable was log-transformed before conducting the formal comparisons. The Levene

test for equal variances and standard model diagnostic procedure were then used to validate the model assumption after the log-transformation. Tukey's Honestly Significant Difference (HSD) method was utilized to control the type I error when conducting multiple pairwise comparisons between group/sex combinations.

To evaluate the statistical significance of differences in mechanoenergetic cost with PAB, sex, and female ovariectomy, a 2 X 3 factorial multivariate Analysis of Variance (MANOVA) was conducted. In the initial analysis, iE_a and iE_{es} (or E_a and E_{es}) were included as two-dimensional dependent variables and the main and interaction effects of PAB, sex and OVX as independent variables. Pairwise comparisons between then 2 X 3 factorial interaction effects were conducted using Tukey's HSD method to control the type I error to be <0.05. To expand on this two-dimensional analysis, we performed another MANOVA with iE_a, iE_{es}, and $\frac{\partial(\boldsymbol{PVA})}{\partial(SV)}$ (or E_a, E_{es}, and $\frac{\partial(\boldsymbol{PVA})}{\partial(SV)}$) as three-dimensional dependent variables and PAB, sex, and OVX as independent variables. All reported P-values are two-sided. Statistical analyses were conducted using IBM SPSS Statistics Version 24 (IBM Corporation, Armonk, NY) and SAS software (SAS Institute, Cary, NC), version 9.4. A p-value of less than 0.05 was considered to be statistically significant.

Results

17β-estradiol levels, body weights, and growth

Ovariectomy in females did not alter bone growth as tibia length was comparable between intact and OVX females (Table 1). Male rats were initially and terminally heavier than female rats regardless of ovariectomy or PAB, and OVX females weighed more than intact female rats at

both timepoints. Over the course of 8 weeks, all rats gained weight with male rats gaining more than female rats. Serum 17β-estradiol levels in males, intact females, and OVX females were within physiological ranges as previously reported(11).

RV estrogen receptor expression

The protective role of estrogen receptors in PAH and pressure overloaded rodent models(11, 14, 15) motivated us to investigate whether transcript levels encoding ERα, ERβ, and Gper1 were sex- or OVX-dependent in the pressure overloaded RV. Only intact female rats demonstrated a decrease in *Esr1* and *Gper1* gene expression in response to PAB (Fig. 2A and C); no significant sex differences were found for *Esr1*, *Esr2*, and *Gper1* transcript levels in response to PAB (Fig. 2A-C). We observed that intact female Shams had greater *Gper1* gene expression levels compared to male Shams. Sex- and OVX-dependent differences in these estrogen receptors therefore are unlikely contributors to sex- or OVX-dependent differences in RV structural or functional responses to PAB.

RV hemodynamics, systemic hemodynamics, and RV hypertrophy

Consistent with the experimental design, PAB generated comparable increases in RV Pes regardless of sex or ovariectomy (Fig. 3A). Heart rate but not SVI decreased post-PAB in the intact animals (Fig. 3B&D). RV ejection fraction (RVEF) was reduced in both the intact and OVX groups (Fig. 3C). Reduced heart rate was a partial contributor to decreased CI (Fig. 3E). In OVX animals, no difference in CI was observed between the sham and PAB groups despite the

decrease in SVI with PAB (Fig. 3D&E). RV hypertrophy was observed in all PAB rats (Fig. 3F), with larger cardiomyocytes in intact females compared to males (Fig. 3G). Systemic pressures measured during open chest right heart catheterization were not different in any group (Table 2). Overall, these findings demonstrate some sex-dependent (larger cardiomyocytes) and some OVX-dependent (smaller CI and SVI) RV structural and functional differences in response to PAB.

RV hemodynamic energy input and output increase with PAB, with the greatest increases in intact females; mechanical efficiency is comparably increased in all PAB groups

We then investigated the effect of sex and ovariectomy on RV hemodynamic energetics with PAB. Energy input, measured by the total (potential plus stroke work) energy generated during contraction (iPVA), was increased in all PAB rats (Fig. 4A). Energy output, measured by energy used during contraction (iEW), also increased in all PAB rats, with the exception that in intact females this increase did not reach statistical significance ($p=0.05$) (Fig. 4B). Intact females demonstrated greater increases in both iPVA and iEW compared to males, however no significant difference was observed with loss of endogenous female sex hormones. As a consequence, the ratio of iPVA to iEW, which is the efficiency of mechanical energy used during contraction, was comparably decreased in all PAB rats, regardless of sex or ovariectomy (Fig. 4C). Thus, while sex and endogenous female sex hormones modulate increases in energy input and output with PAB, mechanical efficiency was not significantly changed.

Effective arterial elastance and end-systolic elastance increase with PAB dependent on sex or ovariectomy; RV mechanoenergetic cost to pump blood is comparably increased in all PAB groups

Like hemodynamic energy input and output and mechanical efficiency, effective arterial elastance (iE_a) and end-systolic elastance (iE_{es}) increased with PAB in females (intact and OVX), and the mechanoenergetic cost to pump blood did not (Fig. 5). However, in males, while iE_a increased with PAB, iE_{es} did not (Fig. 5B). Also, unlike hemodynamic energy input, iE_a had the greatest increase in the OVX females (Fig. 5A) and iE_{es} increased more in OVX females than intact females on average but the change was not significant because of high variability (Fig. 5B). Since iE_a and iE_{es} are independent variables in the calculated RV mechanoenergetic cost to pump blood, we performed a 3D analysis (Fig. 5C) and used MANOVA to determine that RV mechanoenergetic cost to pump blood was increased in all PAB rats ($p<0.05$), but did not significantly change based on sex or ovariectomy. Representative pressure-volume curves for each group are provided in Fig. 5D.

We also confirmed that the results of this analysis do not depend on normalizing E_a, E_{es}, and mechanoenergetic cost to deliver blood to bodyweight (Fig. 6A-C). When these parameters are not normalized, E_a was increased in all PAB rats with the greatest increase in the OVX females (Fig. 6A) and E_{es} was increased significantly in intact and OVX females (Fig. 6B).

RV mitochondrial ultrastructure and PGC-1α transcription levels in response to PAB are not dependent on sex or ovariectomy

We next investigated whether the impact of sex and ovariectomy on energy input was mediated by mitochondrial ultrastructure. RV tissue from intact female demonstrated increased number of mitochondria that corresponded with comparable decrease in mitochondrial size (Fig. 7B&C). Interestingly, male rats also exhibited a significant decrease in mitochondrial size with no significant change in mitochondrial content. As mitochondrial structural remodeling is regulated by PGC-1α(26), we evaluated for sex differences in PGC-1α transcription levels and found that intact female and male rats had comparable downregulation of PGC-1α with PAB (Fig. 7D). While ovariectomy alone reduced PGC-1α transcription level in sham rats, mitochondrial number and size were not significantly altered (Fig. 7B-D). Furthermore, in response to PAB, mitochondrial number, mitochondrial size, and PGC-1α transcription level in OVX PAB rats were not different from OVX sham rats or intact female PAB rats (Fig. 7B-D). Taken together, mitochondrial ultrastructure and PGC-1α transcription levels in response to PAB were largely independent of sex and female sex hormone depletion and did not correspond with changes seen in hemodynamic energy input or RV systolic function.

RV collagen content and collagen organization are affected by sex and ovariectomy; RV diastolic function is comparably impaired in all PAB groups

Since collagen accumulation can impair diastolic function(36), we investigated sex differences in (1) interstitial collagen content and (2) the ratio of thick collagen fibers, which contribute to material stiffness, to thin collagen fibers, which contribute to compliance(17). While RV collagen content was increased in all PAB rats, the increase was significantly smaller in female rats independent of ovariectomy (Fig. 8A). In male and ovariectomized female rats with PAB, the increased ratio of thick-to-thin collagen indicated more packing of collagen fibers into thick

collagen bundles (Fig. 8B). In contrast, intact female rats with PAB had a preserved ratio, suggesting more of thin collagen bundles accumulated. These results indicate that in response to PAB, sex impacts the degree of collagen deposition and loss of endogenous female sex hormones impacts the organization of collagen fibers.

Interestingly, these differences in collagen organization were not demonstrated to be associated with diastolic dysfunction. Regardless of sex or ovariectomy, all PAB rats demonstrated comparable RV chamber stiffening (reduced chamber compliance) and prolonged active relaxation (increased Tau Weiss) (Fig. 8C&D). RV myocardial stiffening was also evident in OVX Sham animals.

Discussion

Our major findings are that, in rats challenged with RV pressure overload via PAB, (1) mechanical efficiency decreased and mechanoenergetic cost to pump blood increased independently of sex, despite differences in hemodynamic energy input, output, and contractility; and (2) diastolic dysfunction occurred independently of sex, despite differences in collagen content and organization. Loss of endogenous sex hormones modulated some of these changes. These data suggest that even though sex and female endogenous sex hormones modulate RV contractile responses and energy input and output responses, the mechanoenergetic cost for the RV to pump blood is not affected by sex or sex hormones. In other words, even though the individual components contributing to RV mechanoenergetic cost are differentially affected by sex and sex hormones in our model, the “end product” of RV mechanoenergetic cost is constant

424 across sexes and after ovariectomy, suggesting a homeostatic target to which the system returns
425 when perturbed. In this case, the target would be maintained mechanoenergetic cost or
426 efficiency.
427
428 In disease states characterized by RV pressure overload, women have superior RV systolic
429 function(10, 16, 45, 50, 53). Preclinical studies in rodent models of PH have recapitulated these
430 clinical findings(11, 25). However, since female sex can alleviate PH-induced pulmonary
431 vascular remodeling(11, 25), sex-dependent changes in RV afterload confound study of the
432 impact of female sex on RV function. Using PAB to induce comparable pressure overload in
433 male and female rats, we confirmed that female rats have greater generation and utilization of
434 mechanical energy (iPVA and iEW), and greater RV contractility (iE_{es}), i.e., improved RV
435 systolic adaptation, compared to male rats. These results are consistent with greater RV
436 contractility found in female PAH patients compared to male PAH patients(50). Interestingly,
437 despite these differences, overall mechanoenergetic function – quantified by both mechanical
438 efficiency and mechanoenergetic cost to pump blood – was not statistically different between the
439 sexes. Although no conclusions can be drawn from the non-significant data shown here, this
440 finding may suggest a sex-independent mechanoenergetic efficiency target that RV systolic
441 adaptation maintains during pressure overload despite mechanoenergetic remodeling pathways
442 that are sex-dependent. It is unknown, however, if both sexes can maintain this
443 mechanoenergetic efficiency for a similar duration. Since male PAH patients have inferior RV
444 adaptation and higher mortality compared to their female counterparts, they may “fall off the
445 cliff” sooner. This may be representative of an intermediate stage of RV adaptation for male rats,
446 implying that there may be some male compensatory response to lower the energetic cost to

pump blood that is not observed in the intact female rats, and may not be sustainable long-term. This idea becomes more intriguing when taken together with the fact that SV and iEes were lower in males compared to intact and OVX females, suggesting a possible sex-dependent compensatory mechanism (or lack thereof) related to RV contractility. However, dedicated time course studies, including an intermediate state of adaptation in males as well as overt RV failure in both males and females, are required to test this hypothesis. To test the hypothesis of a mechanoenergetic efficiency homeostatic set point, one could disrupt cardiomyocyte energetics (e.g., mitochondrial energy generation) constitutively and then observe whether mechanoenergetic efficiency was still maintained at baseline and with pressure overload.

We further explored sex differences by studying the effect of female sex hormone depletion. Menopause is a risk factor for PAH development in patients with scleroderma(44) and more favorable hemodynamics in PAH are seen in women <45 years old(54), which suggest that loss of female sex hormones (e.g. menopause) impairs RV systolic adaptation to PH. Moreover, estrogen therapy has been shown to contribute to improved RV function in ovariectomized rodents with PH(11, 25, 27). Here we found that loss of endogenous sex hormones limited the increase in generation and utilization of mechanical energy during contraction with no significant effect on RV contractility. Again, despite these differences, mechanical efficiency was not altered by loss of endogenous sex hormones. While not significant, the mechanoenergetic cost to pump blood was higher in the OVX group. Since the OVX PAB group had the most anesthesia-related death, loss of data from these sickest animals may have artefactually decreased mechanoenergetic cost to pump blood, which warrants further investigation.

To discover the underlying mechanisms contributing to superior female energy generation and contractility in response to pressure overload, we measured mitochondrial ultrastructure and PGC-1α transcription levels with PAB. While sex differences in mitochondrial ultrastructure and PGC-1α expression level in healthy LV have been reported(7, 23), we found no differences between Sham males and females. We also did not find differences in mitochondrial number or size between Sham males and females, consistent with prior data showing mitochondrial oxidative capacity is independent of sex(2, 6, 23, 41). In response to pressure overload in intact males and females, mitochondrial number increased, mitochondrial size decreased, and PGC-1α transcription decreased, demonstrating sex independence. These changes were generally lost with OVX, suggesting some dependence on endogenous female sex hormones. The regulation of mitochondrial function and energetics is a complex process involving multiple regulators(34, 38), and regulators that were not studied here may be altered. Future studies investigating additional regulators and dissecting time courses are needed. Importantly, these changes in mitochondrial function and energetics do not explain sex-dependent differences in hemodynamic energy input, output and contractility.

In the pressure overloaded LV, sex differences in diastolic dysfunction have been linked with increased rate of collagen deposition(39). Greater ratio of thick to thin collagen fibers and hypertrophy both appear to contribute to myocardial stiffening and diastolic dysfunction in both pressure overloaded ventricles(17, 29, 36). However, sex differences in these features and their resulting contribution to diastolic dysfunction have not yet been investigated. Here, we demonstrate sex differences in collagen content and organization with PAB that nevertheless do not cause sex differences in diastolic stiffening or dysfunction. Males showed more collagen

content and higher thick-to-thin collagen ratio, whereas females had a smaller increase in collagen content with no change in thick-to-thin collagen ratio. Interestingly, OVX females had comparable collagen content to intact females with a greater thick-to-thin collagen ratio. Despite these differences in structure, diastolic function was comparably impaired in all groups with pressure overload. Thus, similar to mechanoenergetic remodeling and systolic function, these results suggest a sex-independent homeostatic set point that governs RV diastolic adaptation to pressure overload achieved via remodeling mechanisms that are sex-dependent.

Study limitations

There are several limitations of this study. First, measurements were made at only one timepoint following a specific degree of PAB such that causal relationships and the relative timing of structural and functional changes in each sex could not be determined. Time courses and different degrees of PAB may result in differential RV energetic responses. It should also be noted that we did not track changes in the pressure gradient across the banded region to ensure consistent levels of banding. However, calculation of pulmonary vascular resistance (Pes/CI) showed comparable amounts of RV afterload with banding across all groups. Second, other factors influenced by sex and loss of endogenous female sex hormones that were not accounted for in this study include oxidative stress(7, 35), calcium handling(8, 9, 43, 51), and inflammation(31). Third, while mitochondrial structure and PGC-1α are strongly linked with mitochondrial function(12, 26), mitochondrial function was not assessed in this study. Fourth, the model-based prediction of cardiac energy cost to deliver blood does not account for some important physiological factors such as heart rate and sympathetic stimulation that are altered

with disease progression. Revision of the modeling approach could enhance its ability to predict ventricular function changes in response to pathological stimuli. Fifth, there was a notable difference in body weight between the intact female and OVX groups at baseline, despite being inbred, from the same vendor, and of the same approximate age, which may confound the comparison between these groups. Finally, the experiments in male rats were conducted two years earlier than those in intact and OVX female rats and by different surgeons. While care and handling of animals, surgical techniques, instrumentation, and data analyses were otherwise identical, comparisons between sexes need to be interpreted with caution.

In conclusion, with the present study, we demonstrate that increases in RV hemodynamic energy generation (input), energy utilization (output), and contractility are greater in females than males whereas mechanical efficiency and mechanoenergetic cost to pump blood are not. Similarly, increases in collagen content and changes in collagen organization are sex-dependent whereas diastolic dysfunction is not. These results point toward sex-dependent mechanisms of remodeling that may be achieved via sex-independent mechanoenergetics and diastolic function, which warrants further investigation.

Conflicting interests

The authors declare that there is no conflict of interest.

Funding

This work was supported by the NIH (grant numbers 1R56HL134736-01A1 to T.L, R01-HL144727-01A1 to T.L., R01-HL-086939 and R01-HL-154624 to N. C. Chesler, T32-HL-007936 to T.-C.Cheng) and VA Merit Review Award (grant number 2 I01 BX002042 to T.L.).

Ethical approval

See methods section.

Guarantor

Not applicable.

Contributorship

All authors made substantial contribution to the study conception, acquisition, analysis, and/or interpretation of the data. Tik-Chee Cheng drafted the manuscript and all authors have critically revised the manuscript for important intellectual content and approved the version to be published.

Acknowledgements

The authors thank Dr. Peiqing Wang, Allison Rodgers, and Randy Massey for technical expertise and valuable help with the surgery, echocardiography, and electron microscopy, respectively. We are grateful to Abigail Drake and Tony So for their help with data collection and analysis.

References

1. **Asanoi H, Kameyama T, Ishizaka S, Nozawa T, and Inoue H**. Energetically optimal left ventricular pressure for the failing human heart. *Circulation* 93: 67-73, 1996.

2. **Barba I, Miro-Casas E, Torrecilla JL, Pladevall E, Tejedor S, Sebastian-Perez R, Ruiz-Meana M, Berrendero JR, Cuevas A, and Garcia-Dorado D**. High-fat diet induces metabolic changes and reduces oxidative stress in female mouse hearts. *J Nutr Biochem* 40: 187-193, 2017.

3. **Betz P, Nerlich A, Wilske J, Wiest I, Penning R, and Eiseumenger W**. Comparison of the solophenyl-red polarization method and the immunohistochemical analysis for collagen type III. *International Journal of Legal Medicine* 105: 27-29, 1992.

4. **Borgdorff MA, Koop AM, Bloks VW, Dickinson MG, Steendijk P, Sillje HH, van Wiechen MP, Berger RM, and Bartelds B**. Clinical symptoms of right ventricular failure in experimental chronic pressure load are associated with progressive diastolic dysfunction. *J Mol Cell Cardiol* 79: 244-253, 2015.

5. **Cheng TC, Philip JL, Tabima DM, Hacker TA, and Chesler NC**. Multiscale structure-function relationships in right ventricular failure due to pressure overload. *American journal of physiology Heart and circulatory physiology* 315: H699-H708, 2018.

6. **Colom B, Oliver J, and Garcia-Palmer FJ**. Sexual Dimorphism in the Alterations of Cardiac Muscle Mitochondrial Bioenergetics Associated to the Ageing Process. *J Gerontol A Biol Sci Med Sci* 70: 1360-1369, 2015.

585 7. **Colom B, Oliver J, Roca P, and Garcia-Palmer FJ**. Caloric restriction and gender
586 modulate cardiac muscle mitochondrial H2O2 production and oxidative damage. *Cardiovasc Res*
587 74: 456-465, 2007.

588 8. **Curl CL, Wendt IR, and Kotsanas G**. Effects of gender on intracellular [Ca2+] in rat
589 cardiac myocytes. *Pflugers Arch* 441: 709-716, 2001.

590 9. **Farrell SR, Ross JL, and Howlett SE**. Sex differences in mechanisms of cardiac
591 excitation-contraction coupling in rat ventricular myocytes. *Am J Physiol Heart Circ Physiol*
592 299: H36-45, 2010.

593 10. **Foppa M, Arora G, Gona P, Ashrafi A, Salton CJ, Yeon SB, Blease SJ, Levy D,**
594 **O'Donnell CJ, Manning WJ, and Chuang ML**. Right Ventricular Volumes and Systolic
595 Function by Cardiac Magnetic Resonance and the Impact of Sex, Age, and Obesity in a
596 Longitudinally Followed Cohort Free of Pulmonary and Cardiovascular Disease: The
597 Framingham Heart Study. *Circ Cardiovasc Imaging* 9: e003810, 2016.

598 11. **Frump AL, Goss KN, Vayl A, Albrecht M, Fisher A, Tursunova R, Fierst J,**
599 **Whitson J, Cucci AR, Brown MB, and Lahm T**. Estradiol improves right ventricular function
600 in rats with severe angioproliferative pulmonary hypertension: effects of endogenous and
601 exogenous sex hormones. *Am J Physiol Lung Cell Mol Physiol* 308: L873-890, 2015.

602 12. **Gomez-Arroyo J, Mizuno S, Szczepanek K, Van Tassell B, Natarajan R, dos**
603 **Remedios CG, Drake JI, Farkas L, Kraskauskas D, Wijesinghe DS, Chalfant CE, Bigbee J,**
604 **Abbate A, Lesnefsky EJ, Bogaard HJ, and Voelkel NF**. Metabolic gene remodeling and

605 mitochondrial dysfunction in failing right ventricular hypertrophy secondary to pulmonary
606 arterial hypertension. *Circ Heart Fail* 6: 136-144, 2013.

607 13. **Hester J, Ventetuolo C, and Lahm T**. Sex, Gender, and Sex Hormones in Pulmonary
608 Hypertension and Right Ventricular Failure. *Comprehensive Physiology* 10: 125-170, 2019.

609 14. **Iorga A, Li J, Sharma S, Umar S, Bopassa JC, Nadadur RD, Centala A, Ren S,**
610 **Saito T, Toro L, Wang Y, Stefani E, and Eghbali M**. Rescue of Pressure Overload-Induced
611 Heart Failure by Estrogen Therapy. *J Am Heart Assoc* 5: 2016.

612 15. **Iorga A, Umar S, Ruffenach G, Aryan L, Li J, Sharma S, Motayagheni N, Nadadur**
613 **RD, Bopassa JC, and Eghbali M**. Estrogen rescues heart failure through estrogen receptor Beta
614 activation. *Biol Sex Differ* 9: 48, 2018.

615 16. **Jacobs W, van de Veerdonk MC, Trip P, de Man F, Heymans MW, Marcus JT,**
616 **Kawut SM, Bogaard HJ, Boonstra A, and Vonk Noordegraaf A**. The right ventricle explains
617 sex differences in survival in idiopathic pulmonary arterial hypertension. *Chest* 145: 1230-1236,
618 2014.

619 17. **Jalil JE, Doering CW, Janicki JS, Pick R, Shroff SG, and Weber KT**. Fibrillar
620 collagen and myocardial stiffness in the intact hypertrophied rat left ventricle. *Circ Res* 64: 1041-
621 1050, 1989.

622 18. **Johnson RC, Datar SA, Oishi PE, Bennett S, Maki J, Sun C, Johengen M, He Y,**
623 **Raff GW, Redington AN, and Fineman JR**. Adaptive right ventricular performance in

response to acutely increased afterload in a lamb model of congenital heart disease: evidence for enhanced Anrep effect. *Am J Physiol Heart Circ Physiol* 306: H1222-1230, 2014.

19. **Junqueira LCU, Montes GS, and Sanchez EM**. The influence of tissue section thickness on the study of collagen by the Picrosirius-polarization method. *Histochemistry* 74: 153-156, 1982.

20. **Kass DA, and Kelly RP**. Ventriculo-arterial coupling: concepts, assumptions, and applications. *Ann Biomed Eng* 20: 41-62, 1992.

21. **Kawaguchi M, Hay I, Fetics B, and Kass DA**. Combined ventricular systolic and arterial stiffening in patients with heart failure and preserved ejection fraction: implications for systolic and diastolic reserve limitations. *Circulation* 107: 714-720, 2003.

22. **Kelly RP, Ting CT, Yang TM, Liu CP, Maughan WL, Chang MS, and Kass DA**. Effective arterial elastance as index of arterial vascular load in humans. *Circulation* 86: 513-521, 1992.

23. **Khalifa AR, Abdel-Rahman EA, Mahmoud AM, Ali MH, Noureldin M, Saber SH, Mohsen M, and Ali SS**. Sex-specific differences in mitochondria biogenesis, morphology, respiratory function, and ROS homeostasis in young mouse heart and brain. *Physiol Rep* 5: 2017.

24. **Kuwabara M, Maruyama H, Onitsuka T, and Koga Y**. Myocardial energetics and cardiac function of preserved rat heart. *Jpn Circ J* 56: 710-715, 1992.

25. **Lahm T, Frump AL, Albrecht ME, Fisher AJ, Cook TG, Jones TJ, Yakubov B, Whitson J, Fuchs RK, Liu A, Chesler NC, and Brown MB**. 17beta-Estradiol mediates superior adaptation of right ventricular function to acute strenuous exercise in female rats with severe pulmonary hypertension. *Am J Physiol Lung Cell Mol Physiol* 311: L375-388, 2016.

26. **Lehman JJ, Boudina S, Banke NH, Sambandam N, Han X, Young DM, Leone TC, Gross RW, Lewandowski ED, Abel ED, and Kelly DP**. The transcriptional coactivator PGC-1alpha is essential for maximal and efficient cardiac mitochondrial fatty acid oxidation and lipid homeostasis. *Am J Physiol Heart Circ Physiol* 295: H185-196, 2008.

27. **Liu A, Schreier D, Tian L, Eickhoff JC, Wang Z, Hacker TA, and Chesler NC**. Direct and indirect protection of right ventricular function by estrogen in an experimental model of pulmonary arterial hypertension. *Am J Physiol Heart Circ Physiol* 307: H273-283, 2014.

28. **Livak KJ, and Schmittgen TD**. Analysis of relative gene expression data using real-time quantitative PCR and the 2(-Delta Delta C(T)) Method. *Methods* 25: 402-408, 2001.

29. **Mendes-Ferreira P, Santos-Ribeiro D, Adao R, Maia-Rocha C, Mendes-Ferreira M, Sousa-Mendes C, Leite-Moreira AF, and Bras-Silva C**. Distinct right ventricle remodeling in response to pressure overload in the rat. *Am J Physiol Heart Circ Physiol* 311: H85-95, 2016.

30. **Montes GS, and Junqueira LC**. The use of the Picrosirius-polarization method for the study of the biopathology of collagen. *Memorias do Instituto Oswaldo Cruz* 86 Suppl 3: 1-11, 1991.

31. **Nadadur RD, Umar S, Wong G, Eghbali M, Iorga A, Matori H, Partow-Navid R, and Eghbali M**. Reverse right ventricular structural and extracellular matrix remodeling by estrogen in severe pulmonary hypertension. *J Appl Physiol (1985)* 113: 149-158, 2012.

32. **Naeije R, Brimioulle S, and Dewachter L**. Biomechanics of the right ventricle in health and disease (2013 Grover Conference series). *Pulm Circ* 4: 395-406, 2014.

33. **Nozawa T, Yasumura Y, Futaki S, Tanaka N, Uenishi M, and Suga H**. Efficiency of energy transfer from pressure-volume area to external mechanical work increases with contractile state and decreases with afterload in the left ventricle of the anesthetized closed-chest dog. *Circulation* 77: 1116-1124, 1988.

34. **Osellame LD, Blacker TS, and Duchen MR**. Cellular and molecular mechanisms of mitochondrial function. *Best Pract Res Clin Endocrinol Metab* 26: 711-723, 2012.

35. **Pavón N, Cabrera-Orefice A, Gallardo-Pérez JC, Uribe-Alvarez C, Rivero-Segura NA, Vazquez-Martínez ER, Cerbón M, Martínez-Abundis E, Torres-Narvaez JC, Martínez-Memije R, Roldán-Gómez FJ, and Uribe-Carvajal S**. In female rat heart mitochondria, oophorectomy results in loss of oxidative phosphorylation. *J Endocrinol* 232: 221-235, 2017.

36. **Rain S, Andersen S, Najafi A, Gammelgaard Schultz J, da Silva Goncalves Bos D, Handoko ML, Bogaard HJ, Vonk-Noordegraaf A, Andersen A, van der Velden J, Ottenheijm CA, and de Man FS**. Right Ventricular Myocardial Stiffness in Experimental

680 Pulmonary Arterial Hypertension: Relative Contribution of Fibrosis and Myofibril Stiffness.
681 *Circ Heart Fail* 9: 2016.

682 37. **Rain S, Handoko ML, Trip P, Gan CT, Westerhof N, Stienen GJ, Paulus WJ,**
683 **Ottenheijm CA, Marcus JT, Dorfmuller P, Guignabert C, Humbert M, Macdonald P, Dos**
684 **Remedios C, Postmus PE, Saripalli C, Hidalgo CG, Granzier HL, Vonk-Noordegraaf A,**
685 **van der Velden J, and de Man FS**. Right ventricular diastolic impairment in patients with
686 pulmonary arterial hypertension. *Circulation* 128: 2016-2025, 2011-2010, 2013.

687 38. **Rosca MG, Tandler B, and Hoppel CL**. Mitochondria in cardiac hypertrophy and heart
688 failure. *J Mol Cell Cardiol* 55: 31-41, 2013.

689 39. **Ruppert M, Korkmaz-Icoz S, Loganathan S, Jiang W, Lehmann L, Olah A, Sayour**
690 **AA, Barta BA, Merkely B, Karck M, Radovits T, and Szabo G**. Pressure-volume analysis
691 reveals characteristic sex-related differences in cardiac function in a rat model of aortic banding-
692 induced myocardial hypertrophy. *Am J Physiol Heart Circ Physiol* 315: H502-H511, 2018.

693 40. **Sagawa K**. *Cardiac contraction and the pressure-volume relationship*. Oxford
694 University Press, USA, 1988.

695 41. **Sanz A, Hiona A, Kujoth GC, Seo AY, Hofer T, Kouwenhoven E, Kalani R, Prolla**
696 **TA, Barja G, and Leeuwenburgh C**. Evaluation of sex differences on mitochondrial
697 bioenergetics and apoptosis in mice. *Exp Gerontol* 42: 173-182, 2007.

698 42. **Schipke JD**. Cardiac efficiency. *Basic Res Cardiol* 89: 207-240, 1994.

699 43. **Schwertz DW, Beck JM, Kowalski JM, and Ross JD**. Sex differences in the response
700 of rat heart ventricle to calcium. *Biol Res Nurs* 5: 286-298, 2004.

701 44. **Scorza R, Caronni M, Bazzi S, Nador F, Beretta L, Antonioli R, Origgi L, Ponti A,**
702 **Marchini M, and Vanoli M**. Post-menopause is the main risk factor for developing isolated
703 pulmonary hypertension in systemic sclerosis. *Ann N Y Acad Sci* 966: 238-246, 2002.

704 45. **Shigeta A, Tanabe N, Shimizu H, Hoshino S, Maruoka M, Sakao S, Tada Y,**
705 **Kasahara Y, Takiguchi Y, Tatsumi K, Masuda M, and Kuriyama T**. Gender Differences in
706 Chronic Thromboembolic Pulmonary Hypertension in Japan. *Circulation Journal* 72: 2069-
707 2074, 2008.

708 46. **Suga H**. Ventricular energetics. *Physiol Rev* 70: 247-277, 1990.

709 47. **Suga H, Hayashi T, and Shirahata M**. Ventricular systolic pressure-volume area as
710 predictor of cardiac oxygen consumption. *Am J Physiol* 240: H39-44, 1981.

711 48. **Suga H, Hayashi T, Suehiro S, Hisano R, Shirahata M, and Ninomiya I**. Equal
712 oxygen consumption rates of isovolumic and ejecting contractions with equal systolic pressure-
713 volume areas in canine left ventricle. *Circ Res* 49: 1082-1091, 1981.

714 49. **Suga H, Igarashi Y, Yamada O, and Goto Y**. Mechanical efficiency of the left
715 ventricle as a function of preload, afterload, and contractility. *Heart Vessels* 1: 3-8, 1985.

50. **Tello K, Richter MJ, Yogeswaran A, Ghofrani HA, Naeije R, Vanderpool R, Gall H, Tedford RJ, Seeger W, and Lahm T**. Sex Differences in Right Ventricular-pulmonary Arterial Coupling in Pulmonary Arterial Hypertension. *Am J Respir Crit Care Med* 2020.

51. **Turdi S, Huff AF, Pang J, He EY, Chen X, Wang S, Chen Y, Zhang Y, and Ren J**. 17-beta estradiol attenuates ovariectomy-induced changes in cardiomyocyte contractile function via activation of AMP-activated protein kinase. *Toxicol Lett* 232: 253-262, 2015.

52. **Vega RB, Konhilas JP, Kelly DP, and Leinwand LA**. Molecular Mechanisms Underlying Cardiac Adaptation to Exercise. *Cell Metab* 25: 1012-1026, 2017.

53. **Ventetuolo CE, Ouyang P, Bluemke DA, Tandri H, Barr RG, Bagiella E, Cappola AR, Bristow MR, Johnson C, Kronmal RA, Kizer JR, Lima JA, and Kawut SM**. Sex hormones are associated with right ventricular structure and function: The MESA-right ventricle study. *American journal of respiratory and critical care medicine* 183: 659-667, 2011.

54. **Ventetuolo CE, Praestgaard A, Palevsky HI, Klinger JR, Halpern SD, and Kawut SM**. Sex and haemodynamics in pulmonary arterial hypertension. *The European respiratory journal* 43: 523-530, 2014.

55. **Vonk-Noordegraaf A, Haddad F, Chin KM, Forfia PR, Kawut SM, Lumens J, Naeije R, Newman J, Oudiz RJ, Provencher S, Torbicki A, Voelkel NF, and Hassoun PM**. Right heart adaptation to pulmonary arterial hypertension: physiology and pathobiology. *J Am Coll Cardiol* 62: D22-33, 2013.

56. **Wang Z, Patel JR, Schreier DA, Hacker TA, Moss RL, and Chesler NC**. Organ-level right ventricular dysfunction with preserved Frank-Starling mechanism in a mouse model of pulmonary arterial hypertension. *Journal of applied physiology* 124: 1244-1253, 2018.

740

741 **Figure Legends**

742 Figure 1. Experimental design and timeline of the described experiments. Pulmonary artery
743 banding (PAB) or sham surgery was performed in age-matched intact male, intact female, and
744 ovariectomized (OVX) female Wistar rats. Eight weeks following surgery, right heart
745 catheterization (RHC) was performed before animals were euthanized for tissue harvest.

746

747 Figure 2. Esr1, Esr2, and Gper1 transcript levels in response to pulmonary artery banding (PAB)
748 are not significantly dependent on sex or ovariectomy. Effects of sex and OVX on (A) Esr1
749 (gene encoding for ERα), (B) Esr2 (gene encoding for ERβ), and (C) Gper1 are shown. N = 8-10
750 animals per group. Values are presented as means ± SEM; $p<0.05$ for *PAB vs. respective sham
751 and †female (intact or OVX) vs. male (2-way ANOVA with Bonferroni's multiple comparison
752 correction).

753

754 Figure 3. Systolic adaptation to pulmonary artery banding (PAB) is independent of sex but
755 dependent on ovariectomy (OVX). Effects of sex and OVX on (A) RV end-systolic pressure
756 (Pes), (B) heart rate (HR), (C) RV ejection fraction (RVEF), (D) stroke volume normalized to
757 bodyweight (SVI), (E) cardiac output normalized to bodyweight (cardiac index), (F) RV weight
758 scaled to left ventricular and septal weights (RV/LV+S), and (G) RV myocyte cross-sectional
759 area (CSA) are shown. (G, left) Representative images depict hematoxylin and eosin stained RV
760 tissue in male and female Sham and PAB rats [hematoxylin staining nuclei in blue, eosin staining
761 cytoplasm in pink]. Note that OVX reduced cardiac index in sham rats. N = 8-10 animals per
762 group. Values are presented as means ± SEM; $p<0.05$ for *PAB vs. respective sham, †female

763 (intact or OVX) vs. male, and ‡OVX vs. intact female (2-way ANOVA with Bonferroni's
764 multiple comparison correction).
765
766 Figure 4. Increases in hemodynamic energy input in response to pulmonary artery banding
767 (PAB) depend on sex and ovariectomy (OVX) but their ratio (mechanical efficiency) does not.
768 Effects of sex and OVX for (A) external work scaled to bodyweight (iEW), (B) pressure volume
769 area scaled to bodyweight (iPVA), and (C) mechanical efficiency (iEW/iPVA) are shown. N = 8-
770 10 animals per group. Values are presented as means ± SEM; $p<0.05$ for *PAB vs. respective
771 sham, †female (intact or OVX) vs. male, and ‡OVX vs. intact female (2-way ANOVA with
772 Bonferroni's multiple comparison correction).
773
774 Figure 5. Increases in indexed RV contractility in response to pulmonary artery banding (PAB)
775 depend on sex and ovariectomy (OVX) but mechanoenergetic cost to pump blood does not.
776 Effects of sex and OVX on (A) indexed arterial elastance (iE_a) and (B) indexed end-systolic
777 elastance (iE_{es}) are shown for each group. N = 8-10 animals per group. Values are presented as
778 means ± SEM; $p<0.05$ for *PAB vs. respective sham, †female (intact or OVX) vs. male, and
779 ‡OVX vs. intact female (2-way ANOVA with Bonferroni's multiple comparison correction). (C)
780 Model-based estimation of RV mechanoenergetic cost to pump blood (change in PVA per unit
781 change in SV) as a function of iE_a and iE_{es}. The group centroid is located at the group average
782 (iE_a, iE_{es}); the boundary is defined by the standard error of mean. PAB groups are significantly
783 different from sham ($p<0.05$) by MANOVA with Tukey's HSD post-hoc test. (D)
784 Representative pressure volume loops recorded during transient vena cava occlusion, from which
785 iE_a and iE_{es} are calculated for each group.

Figure 6. Increases in (non-indexed) RV contractility in response to pulmonary artery banding (PAB) depend on sex and ovariectomy (OVX) but mechanoenergetic cost to pump blood does not. Effects of sex and OVX on (A) arterial elastance (E_a) and (B) end-systolic elastance (E_{es}) are shown for each group. N = 8-10 animals per group. Values are presented as means ± SEM; $p<0.05$ for *PAB vs. respective sham, †female (intact or OVX) vs. male, and ‡OVX vs. intact female (2-way ANOVA with Bonferroni's multiple comparison correction). (C) Model-based estimation of RV mechanoenergetic cost to pump blood (change in PVA per unit change in SV) as a function of E_a and E_{es}. The group centroid is located at the group average (E_a, E_{es}); the boundary is defined by the standard error of mean. PAB groups are significantly different from sham ($p<0.05$) by MANOVA with Tukey's HSD post-hoc test.

Figure 7. RV mitochondrial remodeling in response to pulmonary artery banding (PAB) is dependent on sex and ovariectomy (OVX). Effects of sex and OVX on (B) mitochondrial content, (C) mitochondrial size, and (D) gene expression of PGC-1α are shown. (A) Representative electron micrographs captured at x25,000 magnification are shown for each groups. Number of mitochondria was calculated as the counted number of mitochondria per high power field (HPF). Mitochondrial size was calculated as the cross-sectional area (CSA) of mitochondria per high power field. Note the significant decrease in PGC-1α expression in OVX Sham rats. N = 8-10 animals per group. Values are presented as means ± SEM; $p<0.05$ for *PAB vs. respective sham and ‡OVX vs. intact female (2-way ANOVA with Bonferroni's multiple comparison correction).

Figure 8. Increases collagen content and changes in organization in response to pulmonary artery banding (PAB) depend on sex and ovariectomy (OVX) but diastolic function does not. Effects of sex and OVX are shown for (A) RV interstitial collagen area, (B) RV collagen organization into thick-to-thin collagen fibers, (C) RV chamber compliance indexed to bodyweight, and (D) tau Weiss. Representative images under (A) brightfield and (B) polarized light were captured at x20 magnification. Collagen was stained with picrosirius red; collagen area was calculated as the ratio of the area positive for collagen (stained in pink and red) to the total tissue area (stained yellow). Thick, tightly packed collagen and thin, loosely aligned collagen were identified as different interference colors under polarized light, with thick collagen defined as areas of yellow, orange, or red color, and thin collagen defined as areas of green color. Note that OVX reduced RV chamber compliance index in sham rats. N = 8-10 animals per group. Values are presented as means ± SEM; $p<0.05$ for *PAB vs. respective sham, †female (intact or OVX) vs. male, and ‡OVX vs. intact female (2-way ANOVA with Bonferroni's multiple comparison correction).

Table 1. Estrogen levels, bodyweights, and bodyweight gain in experimental groups.

Parameter	Sham			PAB		
	Intact Male	Intact Female	OVX Female	Intact Male	Intact Female	OVX Female
Tibia length (mm)	-	44.3 ± 0.9	47.0 ± 1.1	-	43.0 ± 0.8	45.4 ± 1.2
Initial bodyweight (g)	267.38 ± 6.46	187.78 ± 4.62†	254.00 ± 7.94‡	262.60 ± 2.35	181.89 ± 4.78†	239.25 ± 8.85†‡
Terminal bodyweight (g)	469 ± 21	272 ± 8†	366 ± 14†‡	455 ± 8	268 ± 8†	346 ± 9†‡
Bodyweight gain (%)	75 ± 6	45 ± 3†	44 ± 3†	73 ± 3	48 ± 2†	45 ± 2†
Serum 17-β Estradiol (pg/mL)	5.27 ± 0.66	14.11 ± 6.58	2.92 ± 0.33	5.82 ± 0.72	7.45 ± 2.13	2.66 ± 0.28

Values are presented as means ± SEM; $p<0.05$ for †female (intact or OVX) vs. male and ‡OVX vs. intact female (2-way ANOVA with Bonferroni's multiple comparison correction).

Table 2. Hemodynamic parameters in sham and pulmonary artery banded (PAB) rats.

	Sham			PAB		
Hemodynamics	Intact Male	Intact Female	OVX Female	Intact Male	Intact Female	OVX Female
Peak Systemic Pressure, mmHg	110 ± 5	116 ± 5	111 ± 8	122 ± 8	119 ± 5	115 ± 8
RV End-diastolic pressure, mmHg	4.50 ± 0.72	3.65 ± 0.38	3.00 ± 0.44	6.48 ± 0.71	6.46 ± 1.28*	4.46 ± 0.84
RV End-systolic volume index, μL/g	0.26 ± 0.03	0.25 ± 0.04	0.24 ± 0.05	0.54 ± 0.04*	0.49 ± 0.09*	0.32 ± 0.07
RV End-diastolic volume index, μL/g	0.94 ± 0.06	0.99 ± 0.11	0.71 ± 0.09	1.04 ± 0.06	1.14 ± 0.11	0.61 ± 0.08†‡

Values are presented as means ± SEM; $p<0.05$ for *PAB vs. respective sham, †female (intact or OVX) vs. male, and ‡OVX vs. intact female (2-way ANOVA with Bonferroni's multiple comparison correction).

Figure 1.

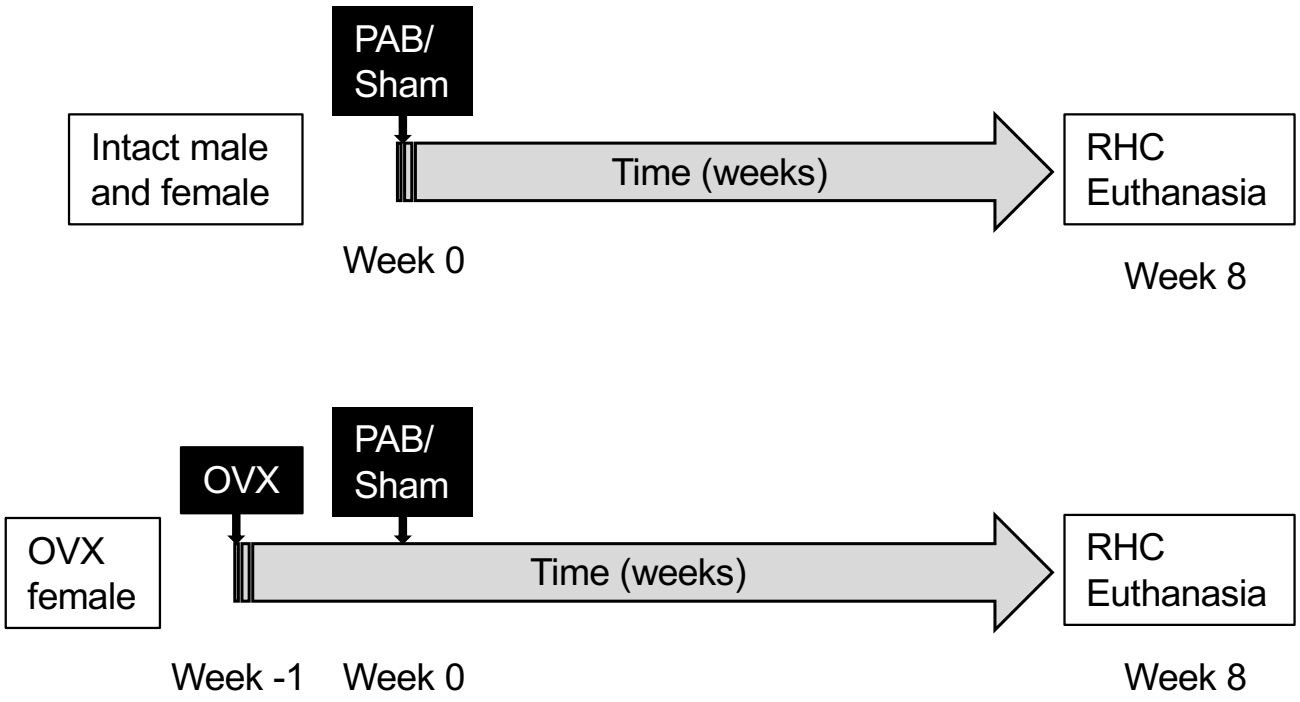
PAB/
Sham
Intact male
and female
Time (weeks)
RHC
Euthanasia
Week 0
Week 8
OVX
PAB/
Sham
OVX
female
Time (weeks)
RHC
Euthanasia
Week -1
Week 0
Week 8

Figure 2.

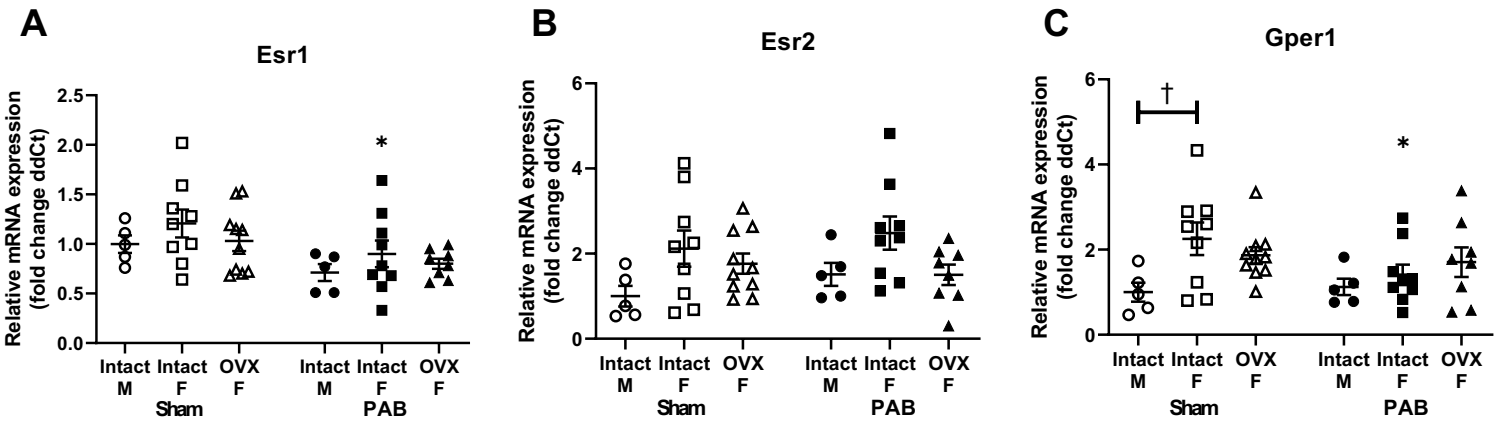
A
Esr1
Relative mRNA expression (fold change ddCt)
2.5
2.0
1.5
1.0
0.5
0.0
*
Intact M
Intact F
OVX F
Intact M
Intact F
OVX F
Sham
PAB
B
Esr2
Relative mRNA expression (fold change ddCt)
6
4
2
0
Intact M
Intact F
OVX F
Intact M
Intact F
OVX F
Sham
PAB
C
Gper1
Relative mRNA expression (fold change ddCt)
6
4
2
0
†
*
Intact M
Intact F
OVX F
Intact M
Intact F
OVX F
Sham
PAB

Figure 3.

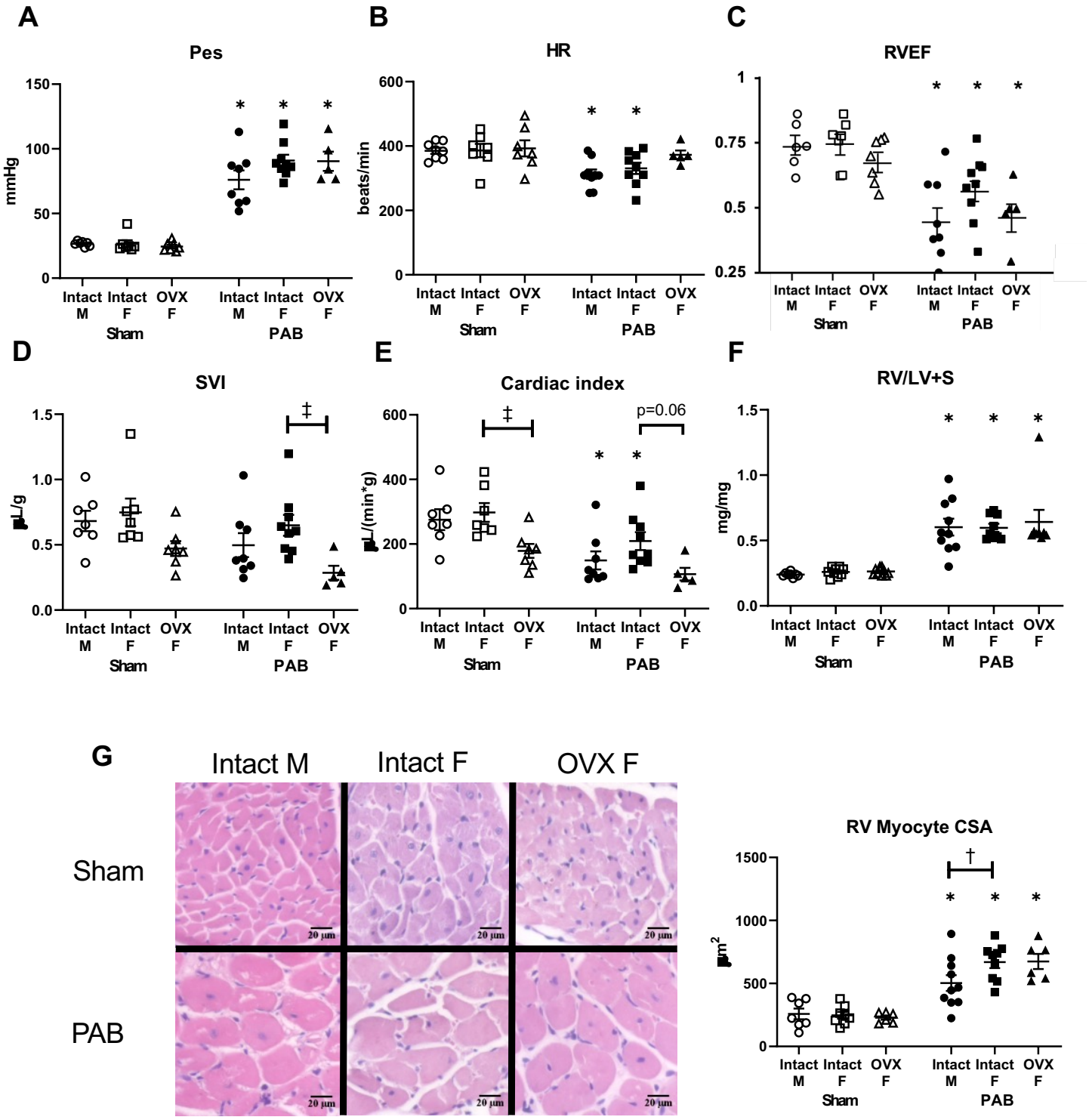
A
Pes
mmHg
150
100
50
0
Intact M
Intact F
OVX F
Sham
PAB
B
HR
beats/min
600
400
200
0
C
RVEF
1
0.75
0.5
0.25
D
SVI
mL/g
1.5
1.0
0.5
0.0
E
Cardiac index
mL/(min*g)
600
400
200
0
‡
p=0.06
F
RV/LV+S
mg/mg
1.5
1.0
0.5
0.0
G
Intact M
Intact F
OVX F
Sham
PAB
20 µm
RV Myocyte CSA
µm2
1500
1000
500
0
†

Figure 4.

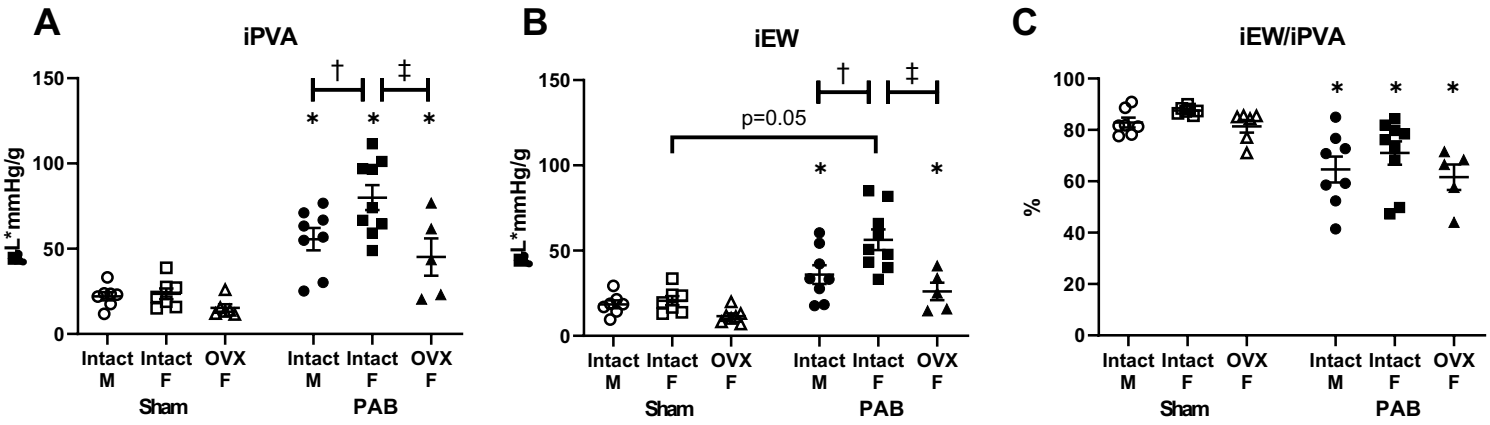
A
iPVA
B
iEW
C
iEW/iPVA
p=0.05
†
‡
*
mL*mmHg/g
%
Intact M
Intact F
OVX F
Sham
PAB

Figure 5.

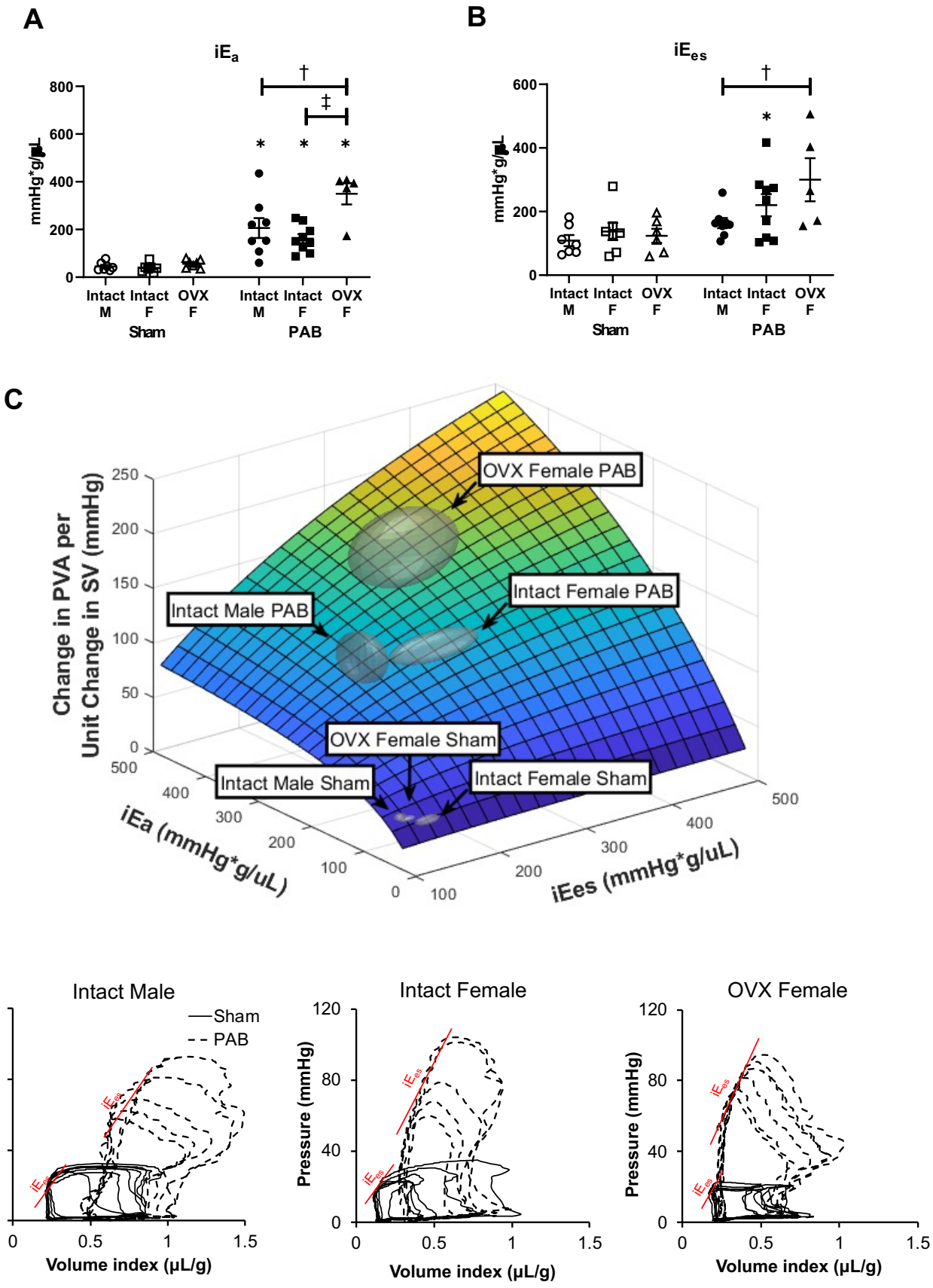
A
iEa
mmHg*g/uL
800
600
400
200
0
†
‡
*
Intact M
Intact F
OVX F
Sham
PAB
B
iEes
600
400
200
0
C
Change in PVA per Unit Change in SV (mmHg)
250
200
150
100
50
0
OVX Female PAB
Intact Female PAB
Intact Male PAB
OVX Female Sham
Intact Male Sham
Intact Female Sham
iEa (mmHg*g/uL)
500
400
300
200
100
0
iEes (mmHg*g/uL)
100
200
300
400
500
D
Intact Male
Intact Female
OVX Female
Sham
PAB
Pressure (mmHg)
120
80
40
0
Volume index (µL/g)
0
0.5
1
1.5

Figure 6.

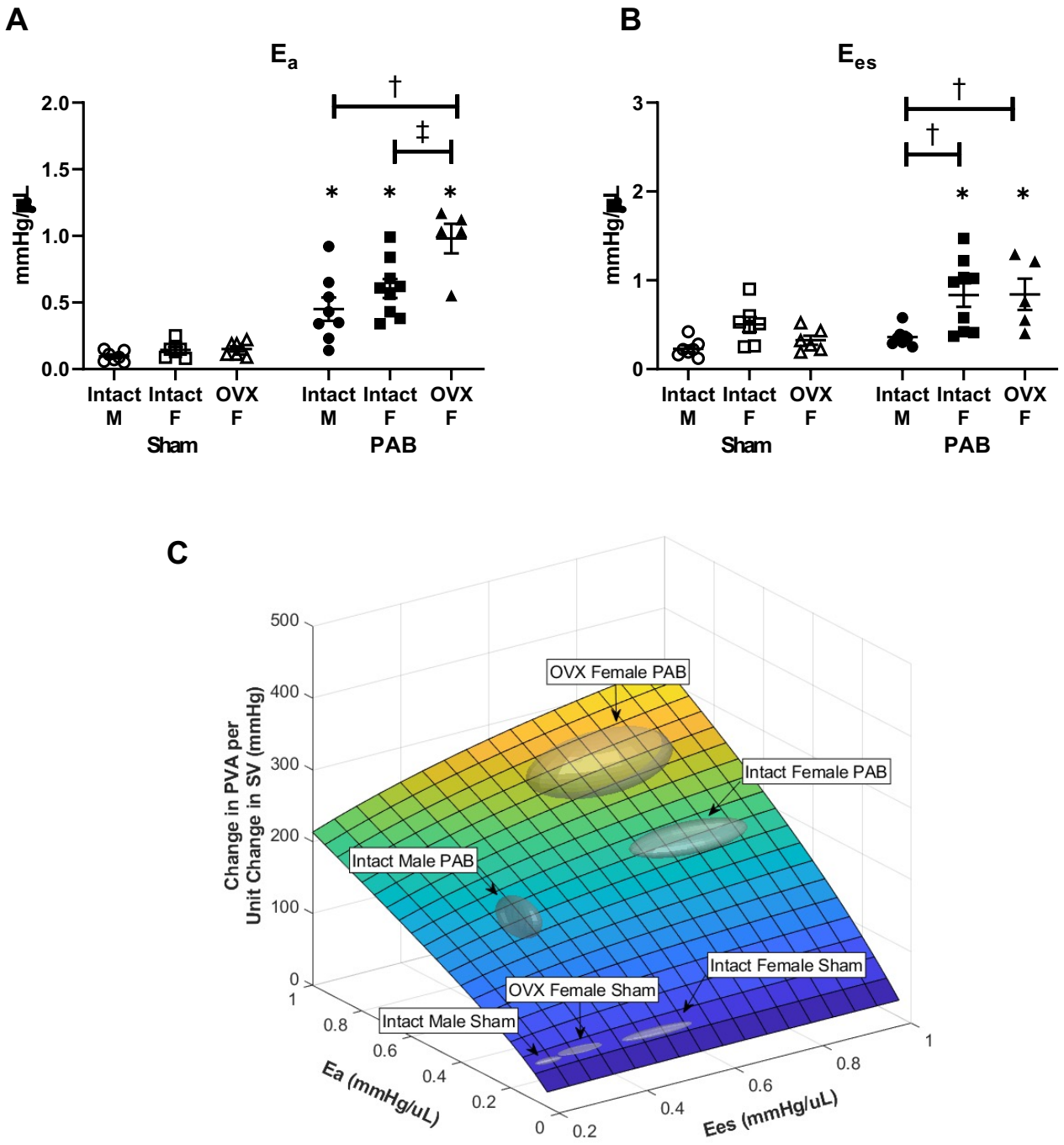
A
E_a
mmHg/uL
2.0
1.5
1.0
0.5
0.0
†
‡
*
Intact M
Intact F
OVX F
Sham
PAB
B
E_{es}
3
2
1
0
C
Change in PVA per Unit Change in SV (mmHg)
500
400
300
200
100
0
OVX Female PAB
Intact Female PAB
Intact Male PAB
Intact Female Sham
OVX Female Sham
Intact Male Sham
Ea (mmHg/uL)
Ees (mmHg/uL)

Figure 7.

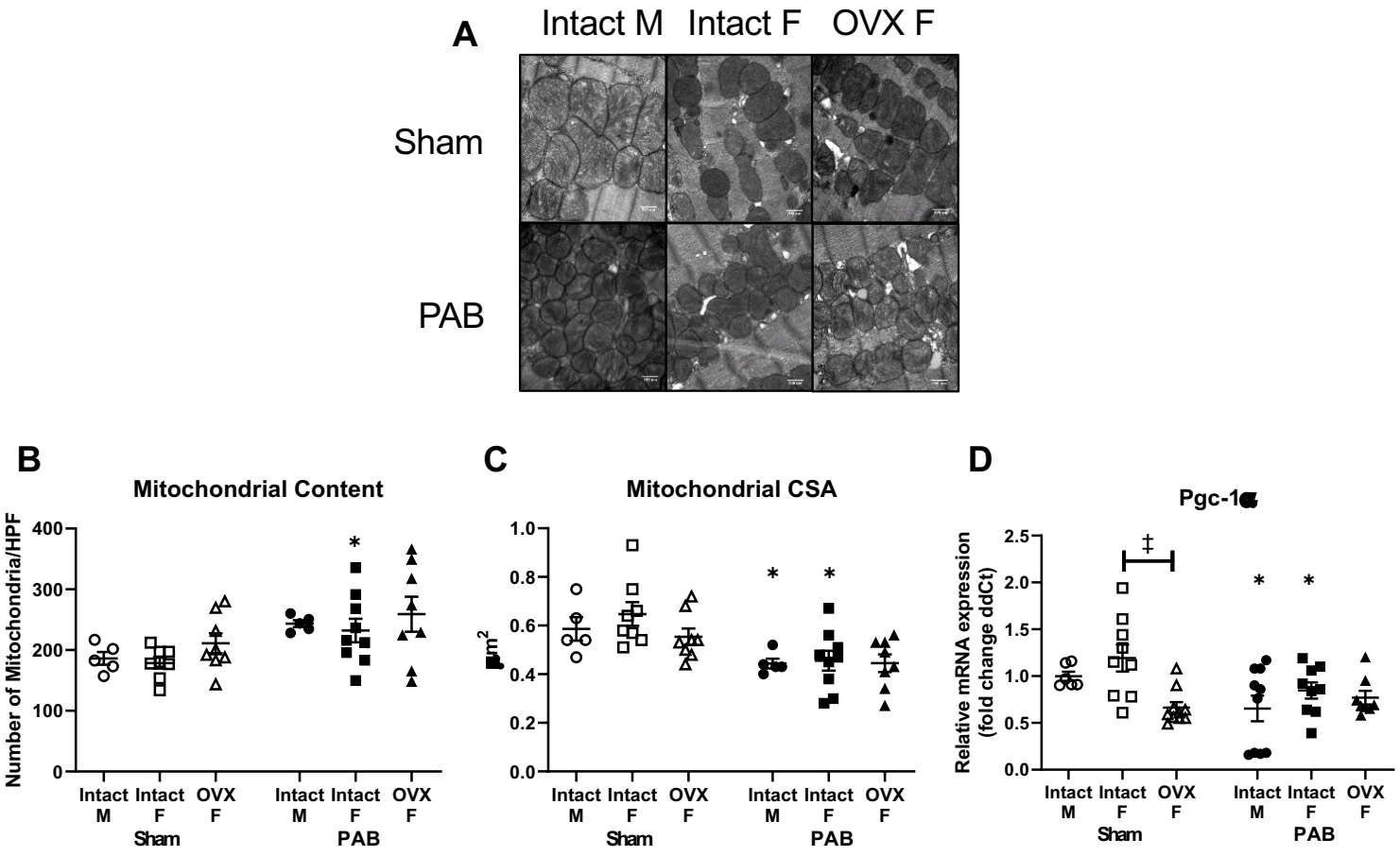
A
Intact M
Intact F
OVX F
Sham
PAB
B
Mitochondrial Content
Number of Mitochondria/HPF
400
300
200
100
0
Intact M
Intact F
OVX F
Intact M
Intact F
OVX F
Sham
PAB
C
Mitochondrial CSA
1.0
0.8
0.6
0.4
0.2
0.0
Intact M
Intact F
OVX F
Intact M
Intact F
OVX F
Sham
PAB
D
Pgc-1α
Relative mRNA expression (fold change ddCt)
2.5
2.0
1.5
1.0
0.5
0.0
Intact M
Intact F
OVX F
Intact M
Intact F
OVX F
Sham
PAB

Figure 8.

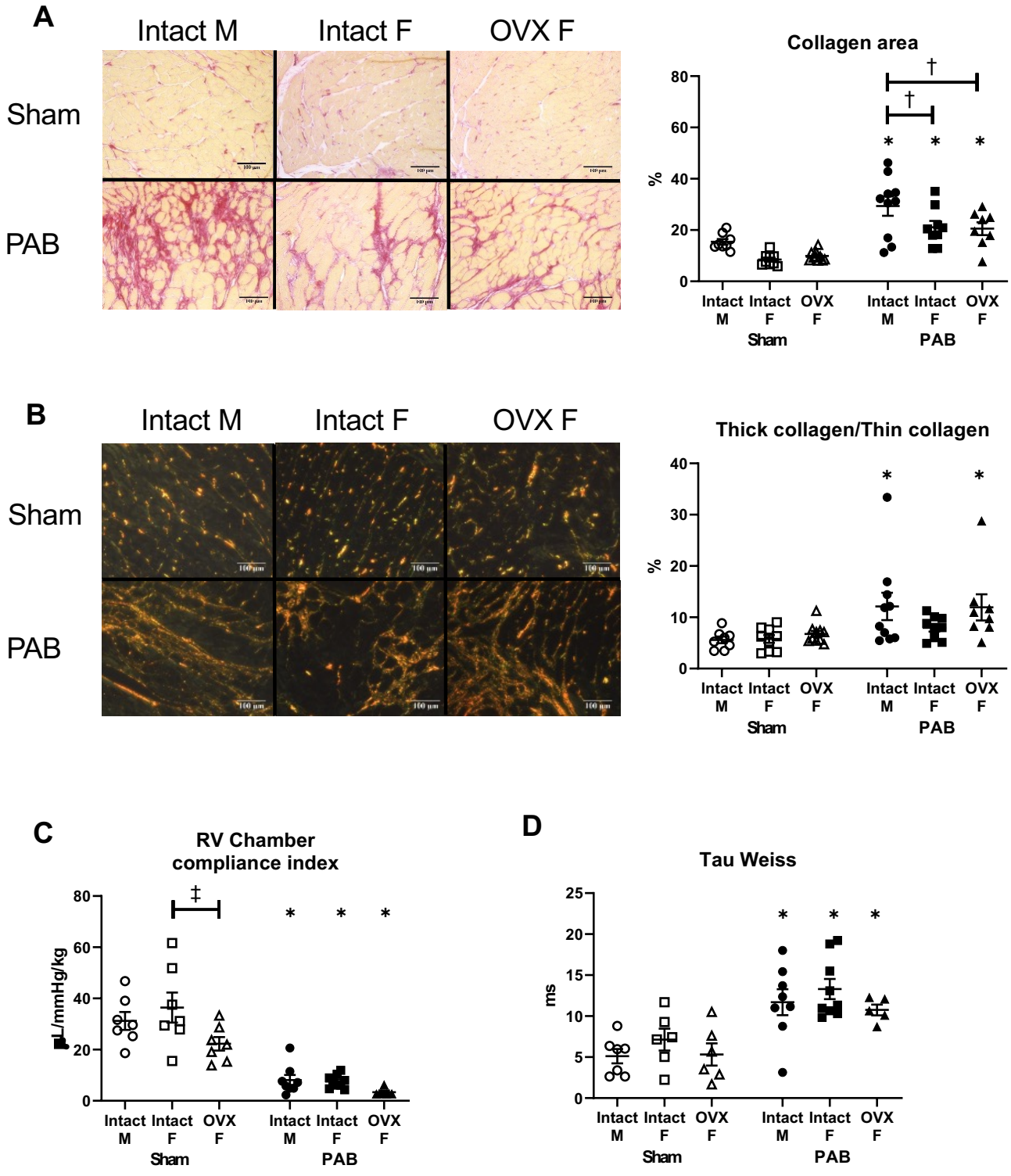
A
Intact M
Intact F
OVX F
Sham
PAB
Collagen area
%
Intact M
Intact F
OVX F
Sham
PAB
B
Thick collagen/Thin collagen
C
RV Chamber compliance index
mL/mmHg/kg
D
Tau Weiss
ms

Sex Differences in Right Ventricular Adaptation to Pressure Overload in a Rat Model

Male, Female, and OVX Female Rats Underwent Pulmonary Arterial Banding for 8 Weeks

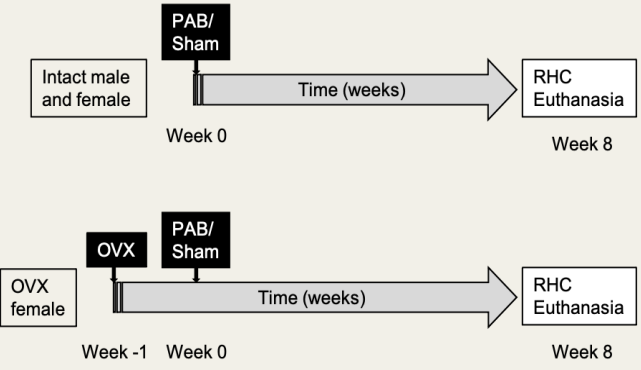

Changes in Remodeling and Hemodynamics were Sex-Dependent while RV Mechanoenergetics and Efficiency Were Sex-Independent

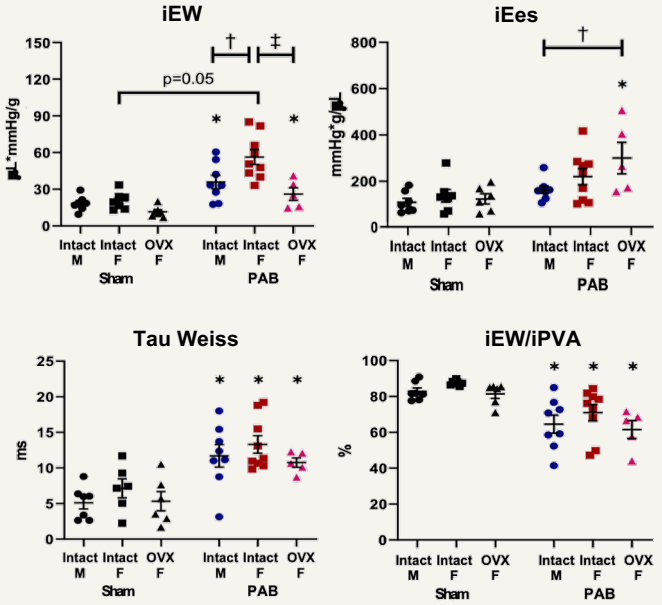

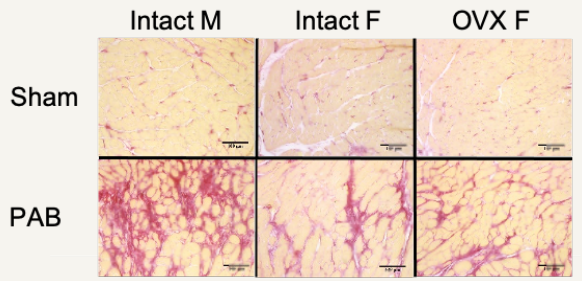

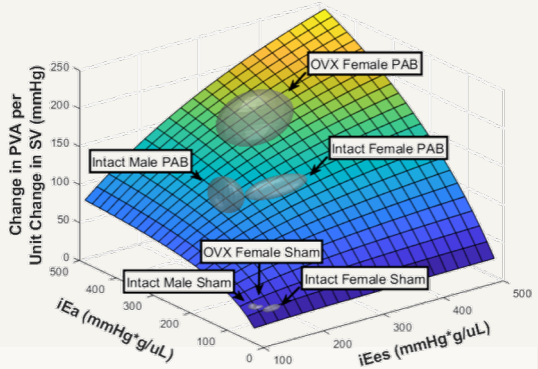

During pressure overload, right ventricle mechanoenergetics are maintained at a sex-independent target via remodeling pathways that are sex-dependent.